ENSO Modulation of the Amazonian Low-Level Jet: More Moisture, Less Rain, and the Role of Land Surface Reception

Ali Bin Shahid

Preprint, May 2026

Author. Ali Bin Shahid

Affiliation. PSKL Water for All, Islamabad 45730, Pakistan

ORCID. 0009-0003-9709-4241

Correspondence. ab.itzhaq@gmail.com

Code. github.com/R3GENESI5/amazon-allj-enso (MIT license)

Archived code. All versions archived under Zenodo concept DOI 10.5281/zenodo.19209347.

Keywords. Amazon basin · Amazonian Low-Level Jet (ALLJ) · ENSO · CHIRPS · ERA5 · GRACE · SMAP · convective triggering · deforestation · land–atmosphere coupling

Preprint disclaimer

Abstract

The Amazonian Low-Level Jet (ALLJ) carries moisture from the tropical Atlantic coast into the basin interior, sustaining wet-season convection. Here we analyze 45 years of ERA5 reanalysis (1979 to 2023), 44 years of CHIRPS precipitation (1981 to 2024), GRACE terrestrial water storage (2002 to 2025), and SMAP root-zone soil moisture (2015 to 2024) to determine how ENSO modulates this transport pathway and its downstream consequences. We find that the ALLJ delivers 15 to 25 percent more moisture during El Nino than during La Nina, yet basin-wide rainfall drops by more than 10 percent. This paradox identifies a convective triggering failure, not a supply failure: the atmosphere contains more moisture but cannot convert it to precipitation because Walker-circulation subsidence suppresses CAPE and shallows the boundary layer. The subsidence anomaly is modest (less than 5 percent of background ascent), indicating that it is necessary but insufficient to explain the full rainfall deficit. Independent satellite observations reveal that deforested land in the arc of deforestation dries approximately 50 percent faster than intact forest following wetting events ($p < 0.001$, SMAP 2015 to 2024), reducing moisture persistence, evapotranspiration, recycling, and the mesoscale soil moisture heterogeneity that promotes convective initiation. We propose a three-lever framework in which Amazon drought is governed by (i) atmospheric moisture supply, (ii) convective triggering, and (iii) land surface water retention. During El Nino, lever (ii) fails while lever (i) strengthens, and lever (iii) compounds the deficit where the land surface is degraded. The ALLJ matters most during El Nino, precisely when the Amazon is most vulnerable.

1. Introduction

The Amazon basin is the largest tropical rainforest on Earth, and its hydrological cycle depends critically on moisture advected from the tropical Atlantic Ocean. Trade winds carry water vapor westward across the basin, sustaining convective rainfall that peaks during the austral summer months of December through February. Within this broad easterly flow, the Amazonian Low-Level Jet (ALLJ) operates as a coherent nocturnal transport mechanism at approximately 900 hPa, present on 10 to 40 percent of wet season nights (Anselmo et al., 2020). The ALLJ concentrates moisture flux into discrete pulses that account for a disproportionate share of total westward moisture transport, making it a central feature of the basin's water budget.

The El Nino-Southern Oscillation (ENSO) is the dominant interannual modulator of Amazon rainfall. During El Nino events, the Amazon basin experiences widespread precipitation deficits, with drought conditions that can persist for months beyond the peak of the oceanic warming (Marengo and Espinoza, 2016). The standard mechanistic explanation invokes Walker circulation dynamics: anomalous subsidence over the Amazon, driven by the eastward shift of the ascending branch of the Walker cell, suppresses deep convection and reduces rainfall (Kousky et al., 1984; Ropelewski and Halpert, 1987). This framework has been broadly successful in explaining the sign and spatial pattern of ENSO-related precipitation anomalies. However, it treats the atmosphere as a unified system in which the supply of moisture and the triggering of convection are implicitly coupled. A critical question remains unresolved. Does El Nino drought in the Amazon arise because the atmosphere delivers less moisture (a supply failure), because the available moisture fails to be converted into rainfall (a triggering failure), or because the land surface cannot retain and recycle the water it receives (a reception failure)? These three mechanisms have distinct implications for understanding drought vulnerability and for predicting how deforestation and climate change will interact in the coming decades. If the drought is primarily a supply failure, then land surface conditions are secondary. If it is a triggering failure, then the factors controlling convective initiation, including boundary layer thermodynamics, surface energy partitioning, and soil moisture heterogeneity (Taylor et al., 2012), become central to the problem. Recent analysis of the record-breaking 2022 to 2024 Amazon drought noted that atmospheric moisture was anomalously high yet convection was inhibited by prevailing atmospheric stability and elevated temperatures (Espinoza et al., 2025). That finding, based on a single

event, suggests the triggering failure mechanism may be general rather than exceptional. Here we test this across the full ENSO cycle using 45 years of reanalysis, isolate the ALLJ as the specific transport mechanism, and add the land surface dimension that event-based studies cannot resolve. This paper builds on earlier work by Shahid and Bunyard (2024), who identified a weakening of the biotic pump mechanism during El Nino years using ERA5 reanalysis. That study demonstrated reduced moisture recycling over the western Amazon but did not separate the contributions of atmospheric supply from land surface reception. Here we extend that analysis by quantifying the ALLJ moisture flux across ENSO phases, comparing it against observed rainfall, and introducing independent satellite-based metrics of land surface water storage.

We use 45 years of ERA5 reanalysis (1979-2023), 44 years of CHIRPS precipitation data (1981-2024), GRACE terrestrial water storage anomalies (2002-2025), and SMAP Level 4 root-zone soil moisture (2015-2024) to test three hypotheses. First, we hypothesize that the ALLJ delivers more moisture to the Amazon basin during El Nino than during La Nina, contrary to the assumption of reduced supply. Second, we hypothesize that rainfall decreases during El Nino despite increased moisture supply, indicating a triggering failure rather than a supply failure. Third, we hypothesize that land surface degradation, particularly in the arc of deforestation along the southern and eastern margins of the basin, independently reduces the capacity of the landscape to retain and recycle moisture, compounding the triggering deficit.

The remainder of this paper is organized as follows. Section 2 describes the datasets and methods. Section 3 presents the climatological moisture flux and its modulation by ENSO. Section 4 documents the triggering paradox: more moisture but less rain. Section 5 evaluates the role of large-scale subsidence. Section 6 examines the diurnal cycle and phase-dependent priming. Section 7 analyzes the precipitation distribution from coast to interior. Section 8 evaluates water storage and land surface reception. Section 9 discusses the three-lever framework and its implications. Section 10 presents the conclusions.

2. Data and Methods

2.1 Datasets

We employ five primary datasets spanning different temporal coverages and spatial resolutions, summarized in Table 1.

Table 1. Summary of datasets used in this study.

Dataset	Variable(s)	Resolution	Period	Reference
ERA5 monthly means of hourly	u, v, q at 900 hPa; omega at 500 hPa	0.25 x 0.25 deg	1979-2023 (45 Februaries)	Hersbach et al. (2020)
ERA5 hourly	u, v, q at 900 hPa; omega at 500 hPa; CAPE, BLH, latent heat flux	0.25 x 0.25 deg	10 selected ENSO years	Hersbach et al. (2020)
CHIRPS v2.0	Monthly precipitation	0.05 x 0.05 deg	1981-2024	Funk et al. (2015)
GRACE/GRACE-FO RL06.3	Terrestrial water storage anomalies (mascon)	~3 deg (mascon)	2002-2025	Watkins et al. (2015)
SMAP L4	Root-zone soil moisture (monthly)	9 km	2015-2024	Reichle et al. (2017)
ONI	Oceanic Nino Index	N/A	1950-present	CPC/NOAA

Note: The 10 ENSO years used for hourly compositing are El Nino: 1983, 1992, 1998, 2010, 2016; La Nina: 1989, 1999, 2000, 2008, 2011.

2.2 Study domain and temporal focus

The study domain spans 6N to 12S latitude and 75W to 40W longitude, encompassing the Amazon basin and the adjacent tropical Atlantic source region. We focus on February, the peak month of the wet season, when both moisture transport and convective activity are at their annual maxima. This choice maximizes the signal-to-noise ratio for detecting ENSO modulation of the moisture transport pathway.

Two sub-regions are defined for comparative analysis. The arc of deforestation (5S to 12S, 55W to 45W) captures the southern and eastern margins of the basin where forest loss has been most extensive since the 1970s. The intact interior (0 to 5S, 65W to 55W) provides a reference region where forest cover has remained largely continuous.

2.3 ENSO classification

We classify years using the Oceanic Nino Index (ONI), defined as the three-month running mean of sea surface temperature anomalies in the Nino 3.4 region (5N-5S, 170W-120W). A February is classified as El Nino if the preceding December-January-February ONI value equals or exceeds +0.5 C, and as La Nina if it equals or falls below -0.5 C. All other years are classified as neutral.

For the hourly compositing analysis, we select the five strongest El Nino Februaries (2016, 1998, 1983, 1992, 2010) and the five strongest La Nina Februaries (1989, 2000, 2008, 1999, 2011) based on ONI magnitude.

2.4 Moisture flux computation

We compute vertically integrated moisture flux at 900 hPa as the product of specific humidity and horizontal wind components:

$$F_u = q \cdot u$$

$$F_v = q \cdot v$$

where *q* is specific humidity (kg kg-1), *u* is the zonal wind component (m s-1), and *v* is the meridional wind component (m s-1). Negative values of F_u indicate westward (into the basin) moisture transport. We compute these fluxes from both the monthly-mean-of-hourly fields (for the full 45-year climatology) and from hourly fields (for the 10-year ENSO composites).

For the nocturnal analysis, we define nighttime hours as 00:00 to 06:00 UTC, corresponding approximately to 21:00 to 03:00 local time across the study domain. This window captures the period of maximum low-level jet intensity, consistent with the nocturnal boundary layer decoupling mechanism described by Anselmo et al. (2020).

The nocturnal fraction of total westward moisture transport is computed at the 52W transect as:

$$f_{noc} = \frac{\sum_{t \in \text{night}} |F_u(t)|}{\sum_{t \in \text{all}} |F_u(t)|}$$

2.5 ENSO compositing and statistical testing

For each variable, we compute El Nino, La Nina, and neutral composites by averaging across all Februaries within each ENSO category. Difference maps (El Nino minus La Nina) are tested for statistical significance using the Welch two-sample t-test at each grid point, with a significance threshold of $p < 0.05$. We report the fraction of grid points within the study domain that exceed this threshold as a measure of spatial coherence.

2.6 Flux retention ratio

To evaluate whether moisture is preferentially rained out at the coast versus transported into the interior, we define a flux retention ratio as the ratio of area-averaged westward moisture flux at 64W to the area-averaged westward moisture flux at 48W. A ratio that does not change across ENSO phases would indicate that moisture passes through the basin without preferential coastal extraction.

2.7 Vertical velocity analysis

Large-scale subsidence is assessed using 500 hPa vertical velocity (omega) from ERA5. In the meteorological convention, positive omega denotes subsidence and negative omega denotes ascent. We compute ENSO composites and difference maps of February-mean omega over the study domain to evaluate the magnitude and significance of Walker circulation anomalies.

3. Climatological Moisture Flux and ENSO Modulation

3.1 Mean state

The 45-year February climatology reveals a persistent westward moisture flux across the Amazon basin at 900 hPa (Fig. 1a). This flux originates over the tropical Atlantic, where trade winds pick up moisture from the warm ocean surface, and extends westward across the basin to the Andean foothills. The strongest fluxes are concentrated between the equator and 5S, aligned with the axis of maximum trade wind convergence. The spatial pattern is consistent with previous descriptions of the low-level moisture transport pathway (Marengo et al., 2004; Vera et al., 2006).

3.2 ENSO modulation of moisture flux

The El Nino minus La Nina difference map shows enhanced westward moisture flux during El Nino across the majority of the study domain (Fig. 1b). This enhancement is statistically significant ($p < 0.05$, Welch's t-test) at 68% of land grid points within the basin. The signal is strongest over the central Amazon between 50W and 60W, where the El Nino composite exceeds the La Nina composite by 15 to 25 percent in zonal moisture flux magnitude.

This result is counterintuitive. The conventional understanding of ENSO impacts on the Amazon emphasizes reduced moisture availability during El Nino (Marengo and Espinoza, 2016). Our analysis shows the opposite: the ALLJ delivers more moisture to the basin during El Nino, not less. The enhanced flux likely reflects stronger Atlantic trade winds during El Nino, driven by the anomalous east-west pressure gradient across the tropical Pacific and Atlantic basins (Wang, 2002; Yoon and Zeng, 2010).

3.3 Nocturnal transport

Hourly composites from the 10 selected ENSO years confirm that nocturnal hours (00:00 to 06:00 UTC) carry a disproportionate share of total westward moisture transport. At the 52W transect, the nocturnal fraction averages 32% of total daily westward moisture flux when computed against the full 24-hour

transport (7 nocturnal hours out of 24). This means that nearly a third of the Amazon's moisture supply arrives during a seven-hour window at night, consistent with the ALLJ mechanism described by Anselmo et al. (2020). When computed against only the nocturnal and daytime windows combined (7 hours each, 14 of 24 hours), the nocturnal share is approximately 52 to 54%, indicating that the ALLJ hours carry slightly more moisture than the equivalent daytime window hour-for-hour. The nocturnal fraction is remarkably stable across ENSO phases: 53.8% during El Nino and 52.7% during La Nina. Note that this comparison uses February 2016 versus February 2021, a case study rather than the multi-year composite; see multi-year composites in Fig. 1 for the robust estimate. This stability indicates that ENSO modulates the total magnitude of moisture transport without altering the diurnal structure of the jet. The ALLJ remains the primary nocturnal transport mechanism regardless of ENSO phase; what changes is how much moisture it carries, not when it carries it.

These findings establish a critical baseline for interpreting the precipitation response. If the atmosphere is delivering more moisture during El Nino, then the observed rainfall deficit cannot be attributed to a supply failure. The cause must lie downstream: in the processes that convert atmospheric moisture into precipitation.

4. The Triggering Paradox: More Moisture, Less Rain

4.1 Precipitation response to ENSO

Despite the enhanced moisture flux documented in Section 3, CHIRPS precipitation data reveal that El Nino Februaries have the lowest rainfall across the entire basin (Fig. 5). This pattern is consistent from the Atlantic coast to the deep interior. At every longitude band from 45W to 70W, El Nino composite precipitation falls below both La Nina and neutral composites.

At the coast (east of 50W), El Nino February precipitation averages 11.6 mm day-1, compared to 13.1 mm day-1 during La Nina. This represents an 11% reduction in rainfall during the phase when moisture supply is highest. In the interior (west of 55W), the deficit is comparable in relative magnitude, indicating that the rainfall suppression is not confined to the coastal zone but extends basin-wide.

4.2 Ruling out coastal rain-out

One possible explanation for the interior drought would be enhanced coastal precipitation during El Nino, effectively intercepting moisture before it reaches the interior. We test this hypothesis using the flux retention ratio, defined as the ratio of westward moisture flux at 64W to that at 48W.

The flux retention ratio does not differ significantly between ENSO phases ($p = 0.72$, Welch's t-test). During El Nino, the ratio is effectively the same as during La Nina, meaning that moisture passes through the coastal zone at similar fractional rates regardless of ENSO state. There is no evidence of preferential coastal rain-out during El Nino. The moisture enters the basin, traverses the coastal zone, and reaches the interior, but it is not converted to rainfall at any point along the transect.

4.3 Implications: triggering failure

The combination of enhanced moisture supply (Section 3) and reduced rainfall (Section 4.1), with no evidence of coastal interception (Section 4.2), points unambiguously to a triggering failure. The atmosphere is loaded with moisture, but the processes that initiate and sustain deep convection are suppressed. This reframes the El Nino drought in the Amazon as fundamentally different from a supply-limited drought. The moisture is present; the atmosphere simply fails to use it.

This distinction has important implications for how we understand land surface feedbacks. If the drought were supply-limited, land surface conditions would be largely irrelevant because the atmosphere would lack the raw material for rainfall regardless of surface state. However, a triggering failure places the land surface at the center of the problem, because convective initiation depends on surface energy fluxes, boundary layer development, and soil moisture heterogeneity (Taylor et al., 2012; Guillod et al., 2015).

5. Subsidence as Necessary but Insufficient

5.1 Vertical velocity composites

The standard explanation for El Nino drought invokes large-scale subsidence over the Amazon driven by the weakened Walker circulation. We evaluate this mechanism using 500 hPa omega composites for February (Fig. 4).

All three ENSO phases maintain net ascent (negative omega) over the Amazon basin. The composite-mean omega values (averaged over 15S to 5S, 70W to 50W) are -0.077 Pa s-1 during El Nino, -0.081 Pa s-1 during La Nina, and -0.085 Pa s-1 during neutral years. The El Nino anomaly relative to the climatological mean is approximately +0.004 Pa s-1: a modest weakening of the ascending motion, not a reversal to subsidence.

This is an important distinction. The Walker circulation anomaly during El Nino does not impose subsidence over the Amazon; it reduces the intensity of the background ascent. The atmosphere over the basin remains convectively unstable in a large-scale sense, with net upward motion at mid-levels maintained across all ENSO phases.

5.2 Spatial significance

The El Nino minus La Nina omega difference is statistically significant at 36% of grid points (including ocean areas; a land-masked estimate would be higher, as in Section 3.2) within the study domain ($p < 0.05$). This is a substantially smaller fraction than the 68% significance found for moisture flux differences (Section 3.2), indicating that the subsidence signal is less spatially coherent than the moisture flux signal. The regions of significant omega anomalies are concentrated over the western Amazon and along the southern margin of the basin, consistent with previous analyses of Walker circulation impacts (Liebmann and Marengo, 2001).

5.3 Subsidence alone cannot explain the drought

The modest magnitude and limited spatial extent of the omega anomalies suggest that Walker circulation weakening is a real but insufficient explanation for the El Nino drought. Several lines of evidence support this conclusion.

First, the omega anomaly (+0.004 Pa s-1) represents less than a 5% change relative to the background ascent, yet the rainfall deficit exceeds 10%. The precipitation response is disproportionate to the large-scale dynamical forcing.

Second, the moisture flux enhancement documented in Section 3 partially compensates for the weakened ascent. More moisture in the column, all else equal, should make convection easier to trigger, not harder. That rainfall decreases despite both enhanced moisture supply and maintained net ascent indicates that additional mechanisms are at work. Third, convective initiation in the tropics depends on surface-based processes that are not captured by 500 hPa omega alone. These include convective available potential energy (CAPE) generated by surface heating and moistening, convective inhibition (CIN) controlled by the boundary layer thermodynamic profile, and mesoscale circulations driven by soil moisture heterogeneity (Taylor et al., 2012). During El Nino, reduced soil moisture and altered surface energy partitioning

could suppress surface-based CAPE, increase CIN, and reduce the mesoscale soil moisture gradients that help trigger afternoon convection. These surface-mediated mechanisms, which we address in Sections 6 through 8, may be the missing link between the modest dynamical anomaly and the disproportionate rainfall response.

In summary, Walker circulation weakening provides a necessary background condition for El Nino drought, but it is not sufficient to explain the magnitude or spatial pattern of the precipitation deficit. The triggering failure documented in Section 4 requires additional mechanisms rooted in land-atmosphere interaction.

The monthly composites in the preceding sections demonstrate that the triggering deficit is real but cannot resolve the sub-daily mechanism. Because the ALLJ is a nocturnal phenomenon, its interaction with daytime convection operates on a timescale that monthly averages obscure. We therefore turn to hourly composites.

6. Diurnal Cycle and Phase-Dependent Priming

The analyses presented in Sections 3 through 5 rely on monthly or daily composites, which obscure the sub-daily structure of moisture transport and convective triggering. Because the ALLJ is fundamentally a nocturnal phenomenon (Anselmo et al., 2020), its interaction with daytime convection operates on a diurnal timescale that monthly averages cannot resolve. We therefore constructed hourly composites from ERA5 for 10 selected ENSO years (five El Nino, five La Nina) to examine the diurnal cycle of moisture flux, CAPE, boundary layer height, and mid-tropospheric vertical velocity.

6.1 Diurnal composites across ENSO phases

Figure 8 presents the mean diurnal cycle of all four variables, composited separately for El Nino and La Nina Februaries. The hourly composites, based on the five strongest ENSO events in each phase, show larger anomalies than the 45-year monthly composites (Section 5) because they sample the extremes of the distribution rather than the full population. The ENSO separation is clear at every hour for every variable, confirming that the phase distinction is not an artifact of temporal averaging.

Moisture flux at 900 hPa peaks during the nocturnal hours (00 to 06 UTC, corresponding to approximately 21 to 03 local time in central Amazonia). This timing is consistent with the known behavior of the ALLJ, which strengthens after sunset as the boundary layer stabilizes and the residual layer decouples from surface friction (Stull, 1988). Both ENSO phases exhibit the same nocturnal peak, but the El Nino composite is consistently higher at all hours. The peak nocturnal moisture flux during El Nino exceeds the La Nina peak by approximately the same margin observed in the monthly composites (Fig. 1), indicating that the enhanced moisture supply is not confined to a narrow time window but persists throughout the diurnal cycle. CAPE shows a pronounced afternoon maximum in both phases, peaking between 18 and 21 UTC (approximately 15 to 18 local time). This is the expected signature of solar heating driving boundary layer destabilization and convective available potential energy accumulation. However, the afternoon CAPE maximum is lower during El Nino than during La Nina, despite the fact that El Nino delivers more moisture to the lower troposphere (Fig. 8b). This result is central to our argument. The atmosphere during El Nino contains more fuel (moisture) but less ability to ignite it (CAPE). The triggering deficit identified in Section 4 is not merely a statistical artifact of monthly composites; it manifests at every hour of the diurnal cycle, with the largest ENSO separation occurring during the afternoon convective maximum.

Boundary layer height provides a physical mechanism for the CAPE suppression. During El Nino afternoons, BLH is shallower than during La Nina, consistent with reduced surface heating and weaker turbulent mixing (Fig. 8c). The shallower boundary layer implies less vigorous thermals, less entrainment of free-tropospheric air, and weaker convective initiation. This is consistent with the enhanced subsidence

documented in Section 5: mid-tropospheric warming associated with anomalous descent stabilizes the free troposphere, raising the level of free convection and reducing the depth of the afternoon mixed layer.

The 500 hPa omega field shows stronger subsidence (less negative omega, indicating weaker upward motion or stronger descent) during El Nino at all hours of the diurnal cycle (Fig. 8d). The diurnal modulation of omega is similar in both phases, with slightly weaker subsidence during afternoon hours when deep convection is most active. The critical observation is that the El Nino subsidence anomaly does not preferentially target a specific time of day; it acts as a persistent baseline suppression that shifts the entire diurnal cycle toward less favorable conditions for deep convection.

6.2 Nocturnal priming of next-day convection

The diurnal composites motivate a more specific question: does nocturnal moisture delivery by the ALLJ influence the convective environment on the following day? If the jet primes the lower troposphere with moisture overnight, this should appear as a lagged correlation between nocturnal moisture flux and next-day CAPE.

Figure 9 presents the results of this priming analysis, computed as Pearson correlations between domain-averaged nocturnal moisture flux (00 to 06 UTC) and domain-averaged CAPE on the following afternoon (18 to 21 UTC), separately for El Nino and La Nina Februaries. The result is the most mechanistically specific finding of this study. During El Nino, nocturnal moisture flux positively correlates with next-day CAPE ($r = +0.18$, $p = 0.03$), indicating that nights with stronger ALLJ transport are followed by afternoons with greater convective potential. During La Nina, the correlation reverses sign ($r = -0.17$, $p = 0.04$), suggesting that additional moisture delivery on already-wet nights is associated with reduced next-day CAPE, possibly through stabilization of the lower troposphere by excessive moisture loading or through nocturnal convection consuming the available instability before the afternoon. The physical interpretation is straightforward. The ALLJ's role in the convective chain is ENSO-phase-dependent. During El Nino, when the atmosphere is moisture-starved relative to its convective potential and subsidence suppresses triggering, the nocturnal moisture pulse from the ALLJ provides a critical increment that partially offsets the triggering deficit. The jet acts as a lifeline, and nights with stronger jet transport are followed by marginally better conditions for daytime convection. During La Nina, when the atmosphere is already near saturation and convective inhibition is weak, additional moisture transport is redundant or counterproductive. The system is already primed, and more fuel does not produce more fire when the ignition system is already operating at capacity.

This asymmetry has implications for seasonal forecasting. During El Nino years specifically, the strength of the ALLJ moisture flux could serve as a useful short-range predictor of next-day convective potential. During La Nina years, other predictors, such as soil moisture heterogeneity (Taylor et al., 2012) or boundary layer convergence patterns, are likely more informative.

7. Precipitation Distribution

This section complements the flux retention ratio analysis in Section 4.2 by using spatially resolved CHIRPS precipitation transects rather than two-point moisture flux comparisons, allowing us to identify where along the coast-to-interior gradient the rainfall deficit is largest.

7.1 Coast-to-interior transects

To determine whether the moisture supply enhancement documented in Sections 3 and 6 translates into spatially uniform or spatially structured precipitation changes, we constructed coast-to-interior precipitation transects from CHIRPS v2.0 monthly data. Transects were extracted along the 0 to 3S latitude band,

spanning from the Atlantic coast (approximately 44W) to the western interior (approximately 72W), and composited by ENSO phase using the ONI classification described in Section 2.

Figure 2 shows the resulting transects for El Nino, La Nina, and neutral Februaries. In all three phases, precipitation decreases from east to west along the transect, consistent with the progressive depletion of Atlantic-sourced moisture as air masses move inland (Eltahir and Bras, 1994; Zemp et al., 2017). The gradient is steepest during El Nino, reflecting the basin-wide precipitation suppression that characterizes drought years.

7.2 Ruling out the coastal rain-out hypothesis

A plausible alternative explanation for the triggering paradox would be that warmer SSTs during El Nino enhance coastal precipitation, effectively spending the additional moisture before it reaches the interior. Under this "ocean rain-out" hypothesis, the interior would experience drought not because of a triggering failure but because the coast intercepts the surplus moisture. The CHIRPS transects allow a direct test.

Figure 2 shows that El Nino suppresses precipitation at all longitudes along the transect, not preferentially at the coast. If ocean rain-out were the dominant mechanism, we would expect coastal precipitation to increase (or at least remain stable) during El Nino while interior precipitation declined. Instead, the suppression is spatially uniform in its sign, with the magnitude of the deficit roughly proportional to the climatological rainfall at each longitude. This pattern is consistent with large-scale subsidence acting across the entire basin, as documented in Section 5, rather than with a coastal boundary layer process that depletes moisture before it penetrates inland.

We therefore conclude that the precipitation deficit during El Nino is basin-wide and dynamically driven, not the result of upstream moisture interception. The additional moisture delivered by the ALLJ during El Nino remains available in the atmospheric column across the full width of the basin. It is not converted to rainfall because the convective triggering mechanism is suppressed, not because the moisture is removed en route.

8. Water Storage and Land Surface Reception

The preceding sections have established that the Amazon drought during El Nino is primarily a convective triggering failure rather than a moisture supply failure. However, this framing addresses only the atmospheric side of the hydrological cycle. The land surface determines what happens to the rainfall that does occur: how much infiltrates, how long it persists in the root zone, how much is recycled to the atmosphere through evapotranspiration, and how much runs off. In this section, we evaluate the land surface reception of moisture using GRACE terrestrial water storage and SMAP root-zone soil moisture.

8.1 GRACE terrestrial water storage

GRACE and GRACE-FO provide monthly estimates of total terrestrial water storage (TWS) anomalies, integrating all water stored in soil, groundwater, surface water, and vegetation. Figure 3 shows the TWS anomaly time series for the Amazon basin from 2002 to 2025. Major storage drops are evident following the El Nino events of 2010, 2016, and 2024, with the 2016 event producing the deepest negative anomaly in the record. The total range of TWS across the study period is approximately 62 cm equivalent water height, indicating substantial interannual variability in basin-scale water storage.

The GRACE record confirms that El Nino events produce basin-wide water deficits that persist for months beyond the end of the oceanic warming. The 2016 event, which was one of the strongest El Nino episodes on record, reduced TWS to a level not observed at any other point in the 23-year satellite record. This is consistent with the triggering deficit mechanism: reduced convective rainfall during the wet season

depletes the water stored in the soil, groundwater, and vegetation compartments, and the deficit carries forward into the subsequent dry season.

8.2 Deforestation signal in water storage trends

To assess whether land surface degradation independently affects water storage, we separated the GRACE record into two sub-domains: the arc of deforestation along the southern and eastern margins of the basin, and the intact forest interior. Figure 6 presents the TWS trends for each sub-domain.

The arc of deforestation shows a declining TWS trend of -0.22 cm/yr over the 2002 to 2025 period, while the intact interior shows a positive trend of +0.43 cm/yr. The difference between these trends is marginally significant ($z = -1.71$, $p = 0.087$), falling just outside the conventional 0.05 threshold but consistent with the expected direction of effect. Neither individual trend reaches conventional significance (arc: $p = 0.17$; intact: $p = 0.21$), reflecting high interannual variability. However, the divergence test has greater power because it targets the difference between co-located regions. The declining trend in the deforested zone is physically plausible: removal of deep-rooted forest reduces infiltration capacity, increases surface runoff, lowers the water table, and reduces dry-season evapotranspiration, all of which reduce the time-averaged water stored in the landscape (Nepstad et al., 1994; Coe et al., 2009).

The marginal significance is not surprising given the coarse spatial resolution of the GRACE mascon product (approximately 3 degrees), which blends deforested and intact areas within each grid cell and dilutes the signal. Higher-resolution datasets are needed to confirm this result, and we turn to SMAP for that purpose.

8.3 SMAP root-zone soil moisture and dry-down rates

SMAP Level 4 provides root-zone soil moisture estimates at 9 km resolution, sufficient to distinguish deforested from intact forest pixels along the southern margin of the basin. We computed e-folding dry-down times from monthly SMAP L4 root-zone soil moisture. For each wetting event (month-over-month increase), we fit an exponential decay to the subsequent declining months and extracted the e-folding time constant. Pixels were separated into two categories: deforested (based on MODIS land cover) and intact closed-canopy forest.

The analysis identified 9 dry-down events in the arc and 10 in the intact interior over the 2015 to 2024 SMAP record. Figure 7 presents the central result. Deforested land dries approximately 50% faster than intact forest following wetting events of comparable magnitude. The difference is highly significant ($p < 0.001$) and robust across years within the 2015 to 2024 SMAP record. The median e-folding time for soil moisture in intact forest is approximately 13.7 months, compared to approximately 8.9 months in deforested areas.

This result has three interconnected consequences for the Amazon hydrological cycle. First, faster dry-down reduces soil moisture persistence, which means that the interval between rainfall events becomes more critical for maintaining vegetation water supply. During El Nino, when the interval between convective events is extended by the triggering deficit, the faster dry-down in deforested areas creates a compounding stress that intact forest does not experience.

Second, reduced soil moisture persistence diminishes evapotranspiration between events. Eltahir and Bras (1994) showed that moisture recycling, the process by which evapotranspiration from the land surface contributes to downwind precipitation, accounts for 25 to 35 percent of total rainfall in the Amazon interior. If deforested land returns less moisture to the atmosphere between events, the recycling fraction declines, and downwind precipitation is reduced. This sets up a positive feedback in which deforestation

at one location reduces rainfall at locations further west along the moisture transport pathway (Zemp et al., 2017).

Third, faster and more uniform drying reduces the mesoscale soil moisture heterogeneity that Taylor et al. (2011, 2012, 2025) have shown to be a driver of convective initiation in the tropics. Convective storms preferentially initiate over boundaries between wet and dry soil patches, where differential surface heating generates mesoscale circulations that lift moist air to the level of free convection. Homogeneous dry surfaces, which are the end state of rapid dry-down over deforested land, produce fewer such boundaries and therefore fewer convective initiation events. The land surface degradation thus reduces not only the supply of moisture to the atmosphere (through reduced evapotranspiration) but also the triggering of convection (through reduced heterogeneity), compounding both sides of the triggering deficit.

The practical implication is that the same rainfall, arriving via the same ALLJ, produces fundamentally different hydrological outcomes depending on the condition of the land surface. Intact forest retains moisture for approximately 50% longer, recycles a larger fraction to the atmosphere, and maintains the spatial heterogeneity that promotes convective initiation. Deforested land allows the same moisture to drain or evaporate rapidly, contributing less to recycling and less to future convective triggering. The land surface is not a passive recipient of atmospheric moisture; it is an active participant in the hydrological cycle, and its degradation weakens the system at every step.

9. Discussion

9.1 The three-lever framework

The results presented in Sections 3 through 8 support a three-lever framework for understanding Amazon drought during El Nino. The three levers are: (i) atmospheric moisture supply via the ALLJ; (ii) convective triggering, governed by CAPE, boundary layer dynamics, and mid-tropospheric stability; and (iii) land surface water retention, determined by vegetation cover, soil properties, and root depth.

Lever (i), moisture supply, is robust across ENSO phases and is actually enhanced during El Nino (Figs. 1, 5, 8). The ALLJ delivers more moisture, not less, during drought years. This finding overturns the implicit assumption in much of the ENSO-Amazon literature that drought reflects reduced atmospheric moisture availability.

Lever (ii), convective triggering, is the primary bottleneck during El Nino events. Subsidence anomalies associated with the Walker circulation shift (Fig. 4) warm the mid-troposphere, stabilize the atmospheric column, suppress afternoon CAPE (Fig. 8), and reduce boundary layer heights. The triggering deficit is present at all hours of the diurnal cycle but is most pronounced during the afternoon convective maximum, when the ENSO separation in CAPE is largest.

Lever (iii), land surface reception, operates on a different timescale. It does not cause the initial precipitation deficit; rather, it determines how quickly the system recovers between events and how much of the received moisture is recycled back to the atmosphere. Deforested land dries approximately 50% faster than intact forest (Fig. 7), reducing moisture persistence, evapotranspiration, recycling, and mesoscale heterogeneity. This lever is degradation-sensitive rather than ENSO-sensitive, meaning that it compounds the triggering deficit regardless of the interannual climate state.

9.2 Revising the standard narrative

The standard narrative of El Nino-driven Amazon drought, as articulated by Marengo and Espinoza (2016) and earlier by Kousky et al. (1984), holds that Walker circulation subsidence suppresses moisture supply and convection simultaneously. Our results show that this account is incomplete in two respects. First,

the subsidence anomaly over the Amazon interior is modest in magnitude (Fig. 4), and the moisture supply actually increases during El Nino, indicating that the Walker circulation affects convective triggering far more than it affects moisture transport. Second, the standard narrative neglects the land surface entirely, treating the Amazon basin as a passive receiver of atmospheric inputs. Our SMAP and GRACE results demonstrate that the land surface is an active and degradation-sensitive component of the drought mechanism.

The revised account is as follows. During El Nino, the eastward shift of the Walker circulation ascending branch produces anomalous subsidence over the Amazon. This subsidence warms the mid-troposphere, increases convective inhibition, and suppresses the afternoon convective cycle. Meanwhile, the ALLJ continues to deliver moisture at or above normal rates, possibly enhanced by stronger Atlantic-to-continent pressure gradients associated with the SST anomaly pattern. The result is a moisture-rich but convectively inhibited atmosphere: more fuel, less ignition. The rainfall that does occur is reduced in frequency and intensity. In deforested areas, this reduced rainfall drains or evaporates approximately 50% faster than in intact forest, leaving the soil drier for longer intervals. The drier soil reduces evapotranspiration, reduces the moisture available for recycling, and homogenizes the surface energy balance, further suppressing convective initiation. The drought is therefore a product of atmospheric triggering failure compounded by land surface retention failure, not of moisture supply failure.

9.3 Connection to the biotic pump framework

Shahid and Bunyard (2024) proposed, building on the biotic pump theory of Makarieva and Gorshkov (2007), that deforestation weakens the atmospheric moisture recycling chain by reducing evapotranspiration and disrupting the pressure gradients that draw moist air from the ocean into the continental interior. Our results provide direct observational support for a specific component of this prediction. The biotic pump framework predicts that land surface degradation should reduce the efficiency of moisture retention and recycling without necessarily reducing the amount of moisture arriving from the Atlantic. This is precisely what we observe.

The SMAP dry-down analysis (Fig. 7) shows that the pump is weakened not because less moisture arrives at the land surface, but because the land cannot hold what arrives long enough to re-evaporate it. The GRACE trends (Fig. 6) show that this retention failure manifests as a declining water storage signal in the arc of deforestation, while the intact interior maintains or slightly increases its storage. The moisture supply chain from ocean to atmosphere to land surface remains intact; the failure occurs at the land surface reception step, where deforestation has degraded the capacity of the landscape to participate in the recycling loop.

9.4 The ALLJ as a dual provider: moisture and wind shear

Taylor et al. (2025) recently demonstrated, using 2.2 million convective events across sub-Saharan Africa, that wind shear amplifies the influence of soil moisture heterogeneity on thunderstorm initiation. Where soil-moisture-driven circulations oppose the direction of shear-induced cloud displacement, vertical storm growth is maximized. A companion study (Barton et al., 2025) extended this to mesoscale convective systems globally, showing that soil moisture gradients spanning hundreds of kilometres can strengthen storms by driving increased vertical wind shear conditions.

The ALLJ is directly relevant to this mechanism. During nocturnal hours, the jet produces persistent low-level wind shear across the Amazon basin through the vertical velocity gradient between the jet core at 900 hPa and the stable surface layer below. In intact forest, where our SMAP analysis (Fig. 7) shows that soil moisture persists for approximately 14 months after wetting events, the landscape sustains the mesoscale

heterogeneity that Taylor et al. (2012) showed drives convective initiation. The ALLJ's wind shear interacts with this heterogeneity to enhance storm development.

In deforested areas, the situation is fundamentally different. Faster drying (approximately 9 months e-folding time) produces more spatially uniform soil moisture conditions. The ALLJ still provides wind shear, but the shear has no heterogeneity to work with. The dual role of the ALLJ, as both moisture supplier and wind shear provider, is therefore contingent on land surface condition. Deforestation breaks the coupling between the jet and the land surface, not by weakening the jet itself, but by removing the surface property that allows the jet's dynamical effects to translate into convective initiation.

This connection has not previously been made for the Amazon and suggests that the three-lever framework may understate the importance of lever (iii): land surface degradation does not merely reduce moisture retention but also disables a dynamical pathway through which the ALLJ supports convection.

A further implication concerns the boundary between cleared and intact land. Deforested areas heat faster than adjacent forest, generating stronger sensible heat flux and mesoscale circulations that draw moisture laterally from the intact canopy. The moisture extracted enters a surface with low holding capacity, drains or evaporates quickly, and exits the recycling loop. The deforestation boundary therefore does not merely fail to contribute to the water cycle; it actively degrades the hydrological function of adjacent intact forest. The scale of the clearing likely determines the outcome: small clearings may produce moisture gradients that trigger convection through the Taylor et al. (2012) mechanism, while large clearings may act as persistent moisture sinks that dehydrate their neighbours. Zemp et al. (2017) modelled this as cascading forest loss, in which reduced ET in one area propagates as reduced rainfall downwind. Our SMAP residence time methodology provides a framework for testing this directly: comparing dry-down rates in intact forest pixels adjacent to deforestation edges versus deep interior forest pixels would reveal whether the boundary effect is measurable at 9 km resolution. This analysis is beyond the scope of the present study but represents a priority for follow-up work.

The three-lever framework can also be expressed in economic terms. The SMAP residence time is, in effect, a depreciation rate for landscape hydrological function. Intact forest depreciates slowly (14-month e-folding time); degraded land depreciates rapidly (9 months). Restoration lengthens the residence time, slowing the depreciation. If the fiscal instruments that currently subsidize activities accelerating land surface degradation (clearing, drainage, conversion to pasture) were redirected toward restoration of infiltration, storage, and ET capacity, the return would be measured not only in local water retention but in the sustained moisture recycling that supports rainfall hundreds of kilometres downwind.

9.5 Implications for forecasting

The phase-dependent priming result (Fig. 9) has specific implications for operational forecasting. During El Nino years, when the atmosphere is moisture-limited relative to its convective potential, the nocturnal ALLJ moisture flux correlates positively with next-day CAPE. This suggests that real-time monitoring of ALLJ strength, which is observable from radiosonde data at Belem and Manaus as well as from reanalysis products, could provide a useful 12 to 24 hour predictor of convective potential. During La Nina years, this predictor would not be informative, and other predictors, including soil moisture state and boundary layer convergence patterns, would be more relevant.

The nocturnal partition map further specifies the spatial envelope within which the ALLJ matters most. The jet's dominance of moisture transport is strongest along the coastal-to-mid-basin corridor, from approximately 44W to 60W, and weakens in the western basin beyond 60W. This defines the geographic region in which ALLJ-based forecasting would have the greatest skill.

9.6 Limitations

Several limitations qualify our findings. First, we restrict our analysis to February, the peak month of the wet season. The ALLJ operates throughout the wet season (November through March), and its ENSO modulation may differ in the shoulder months when the background convective environment is weaker. Extension to the full wet season is a priority for future work.

Second, the SMAP record spans only 10 years (2015 to 2024), limiting our ability to assess long-term trends in soil moisture dynamics. The dry-down rate difference between deforested and intact forest is highly significant within this period, but we cannot determine whether it has been changing over time as deforestation has progressed.

Third, the GRACE spatial resolution (approximately 3 degrees for the mascon product) is coarse relative to the spatial scale of deforestation. The marginally significant trend difference between the arc of deforestation and the intact interior ($p = 0.087$) may reflect signal dilution rather than a weak underlying effect. Higher-resolution gravimetry from future missions would help resolve this ambiguity.

Fourth, the priming correlation, while statistically significant in both ENSO phases, explains only approximately 3 percent of the variance in next-day CAPE (r squared of approximately 0.03). The ALLJ moisture flux is one input among many that determine the convective environment, and its predictive value should not be overstated. The significance of the result lies in the sign reversal between ENSO phases, which reveals the phase-dependent role of the jet, rather than in the magnitude of the explained variance.

Fifth, we do not account for aerosol effects on convection. Biomass burning in the arc of deforestation produces substantial aerosol loading during the dry season and the transition to the wet season (Artaxo et al., 2002), which can modify cloud microphysics and suppress or delay convective rainfall (Andreae et al., 2004). This mechanism may interact with the triggering deficit documented here, particularly in the deforested zone where fire activity is concentrated.

10. Conclusions

This study presents a multi-dataset analysis of the Amazonian Low-Level Jet and its interaction with ENSO, convective triggering, and land surface water retention during the peak wet season month of February. Three key findings emerge.

First, the ALLJ delivers more moisture to the Amazon basin during El Nino than during La Nina. This result, established from 45 years of ERA5 reanalysis and confirmed in hourly diurnal composites (Figs. 1, 5, 8), overturns the assumption that El Nino drought in the Amazon reflects reduced atmospheric moisture supply. The moisture delivery mechanism is robust; it strengthens rather than weakens during drought years.

Second, the Amazon drought during El Nino is a convective triggering deficit, not a moisture supply deficit. Despite enhanced moisture availability, CAPE is lower, boundary layers are shallower, and mid-tropospheric subsidence is stronger during El Nino (Figs. 4, 8). The atmosphere contains more fuel but cannot release it. The precipitation deficit is basin-wide and cannot be explained by coastal rain-out or upstream moisture interception (Fig. 2). The nocturnal priming analysis (Fig. 9) reveals that the ALLJ's contribution to convective potential is ENSO-phase-dependent: it is the critical moisture lifeline during El Nino drought years and largely redundant during La Nina wet years.

Third, land surface degradation independently reduces water retention, with deforested land drying approximately 50% faster than intact forest after wetting events (Fig. 7). This faster dry-down reduces soil moisture persistence, diminishes evapotranspiration and moisture recycling (Eltahir and Bras, 1994), and homogenizes the surface energy balance in ways that suppress convective initiation (Taylor et al., 2012).

GRACE terrestrial water storage trends suggest a declining trajectory in the arc of deforestation that is absent in the intact interior (Fig. 6), though this result is only marginally significant at the resolution of the current satellite record.

The practical implication of these findings is that intervention strategies for Amazon drought resilience should prioritize land surface restoration over atmospheric modification. The atmosphere delivers moisture reliably, even during El Nino events. The land surface determines whether that moisture is retained long enough to sustain vegetation, recycle to the atmosphere, and contribute to downwind rainfall. Investments in infiltration capacity, vegetation cover, soil organic matter, and the maintenance of landscape heterogeneity address the lever that is both most degraded and most amenable to human action. The atmospheric triggering deficit during El Nino is a climatic given; the land surface reception deficit is a consequence of land use decisions that can, in principle, be reversed.

The ALLJ's role in this system is asymmetric. It matters most precisely when the Amazon is most vulnerable: during El Nino drought years, when convective triggering is suppressed and every increment of moisture to the lower troposphere provides a marginal benefit to the convective environment. During La Nina years, the jet's contribution is largely redundant, as the system is already near saturation. This phase-dependent asymmetry means that the ALLJ is not merely a transport mechanism to be characterized climatologically; it is a drought-sensitive lifeline whose importance varies with the state of the coupled ocean-atmosphere-land system.

Data and Code Availability

All datasets used in this study are openly available.

- **ERA5 reanalysis** (Copernicus Climate Data Store):
  - Monthly means on pressure levels (Hersbach et al. 2023a, doi:10.24381/cds.6860a573)
  - Hourly on pressure levels (Hersbach et al. 2023b, doi:10.24381/cds.bd0915c6)
  - Hourly on single levels (Hersbach et al. 2023c, doi:10.24381/cds.adbb2d47)
  - Methodology: Hersbach et al. (2020), doi:10.1002/qj.3803
- **CHIRPS v2.0** monthly precipitation, UCSB Climate Hazards Center: https://data.chc.ucsb.edu/products/CHIRPS-2.0/ (Funk et al. 2015, doi:10.1038/sdata.2015.66)
- **GRACE/GRACE-FO JPL RL06.3 V4 mascons** (CRI-filtered), NASA PO.DAAC: doi:10.5067/TEMSC-3JC634; methodology in Watkins et al. (2015), doi:10.1002/2014JB011547
- **SMAP L4 SPL4SMGP v8** root-zone soil moisture, NASA NSIDC DAAC: doi:10.5067/T5RUATAQREF8; product evaluation in Reichle et al. (2017), doi:10.1175/JHM-D-17-0063.1
- **Oceanic Niño Index** (no dataset DOI), NOAA Climate Prediction Center: https://origin.cpc.ncep.noaa.gov/product

All analysis code that produces the figures in this paper is openly available at https://github.com/R3GENESI5/amazon-allj-enso, released under the MIT license. All versions archived under Zenodo concept DOI 10.5281/zenodo.19209347.

References

Andreae, M. O., Rosenfeld, D., Artaxo, P., Costa, A. A., Frank, G. P., Longo, K. M., & Silva-Dias, M. A. F. (2004). Smoking rain clouds over the Amazon. *Science*, 303(5662), 1337-1342.

Anselmo, E. M., Schumacher, C., & Machado, L. A. T. (2020). The Amazonian low-level jet and its connection to convective cloud organization and propagation. *Monthly Weather Review*, 148(10), 4065-4082.

Anselmo, E. M., Schumacher, C., & Machado, L. A. T. (2021). The interaction between the nocturnal Amazonian low-level jet and convection in CESM. *Journal of Climate*, 34(21), 8665-8680.

Artaxo, P., Martins, J. V., Yamasoe, M. A., Procopio, A. S., Pauliquevis, T. M., Andreae, M. O., Guyon, P., Gatti, L. V., & Leal, A. M. C. (2002). Physical and chemical properties of aerosols in the wet and dry seasons in Rondonia, Amazonia. *Journal of Geophysical Research: Atmospheres*, 107(D20), 8081.

Coe, M. T., Costa, M. H., & Soares-Filho, B. S. (2009). The influence of historical and potential future deforestation on the stream flow of the Amazon River. *Journal of Hydrology*, 369(1-2), 165-174.

Barton, E. J., Klein, C., Taylor, C. M., & Burns, H. (2025). Soil moisture gradients strengthen mesoscale convective systems by increasing wind shear. *Nature Geoscience*, 18, 330-336. doi:10.1038/s41561-025-01666-8.

Eltahir, E. A. B., & Bras, R. L. (1994). Precipitation recycling in the Amazon basin. *Quarterly Journal of the Royal Meteorological Society*, 120(518), 861-880.

Espinoza, J. C., et al. (2025). Moisture and temperature sources were key drivers of the anomalies for the record-breaking of 2023 Amazon drought. *Communications Earth and Environment*. doi:10.1038/s43247-025-02771-7.

Funk, C., Peterson, P., Landsfeld, M., Pedreros, D., Verdin, J., Shukla, S., Husak, G., Rowland, J., Harrison, L., Hoell, A., & Michaelsen, J. (2015). The climate hazards infrared precipitation with stations: A new environmental record for monitoring extremes. *Scientific Data*, 2, 150066.

Guillod, B. P., Orlowsky, B., Miralles, D. G., Teuling, A. J., & Seneviratne, S. I. (2015). Reconciling spatial and temporal soil moisture effects on afternoon rainfall. *Nature Communications*, 6, 6443.

Hersbach, H., Bell, B., Berrisford, P., Hirahara, S., Horanyi, A., Munoz-Sabater, J., Nicolas, J., Peubey, C., Radu, R., Schepers, D., Simmons, A., Soci, C., Abdalla, S., Abellan, X., Balsamo, G., Bechtold, P., Biavati, G., Bidlot, J., Bonavita, M., … Thepaut, J.-N. (2020). The ERA5 global reanalysis. *Quarterly Journal of the Royal Meteorological Society*, 146(730), 1999-2049.

Shahid, A. B., & Bunyard, P. P. (2024). In defence of the biotic pump. *Journal of Atmospheric Science Research*, 8(1), 41-64.

Kousky, V. E., Kagano, M. T., & Cavalcanti, I. F. A. (1984). A review of the Southern Oscillation: Oceanic-atmospheric circulation changes and related rainfall anomalies. *Tellus A*, 36(5), 490-504.

Liebmann, B., & Marengo, J. A. (2001). Interannual variability of the rainy season and rainfall in the Brazilian Amazon basin. *Journal of Climate*, 14(22), 4308-4318.

Makarieva, A. M., & Gorshkov, V. G. (2007). Biotic pump of atmospheric moisture as driver of the hydrological cycle on land. *Hydrology and Earth System Sciences*, 11(2), 1013-1033.

Marengo, J. A., & Espinoza, J. C. (2016). Extreme seasonal droughts and floods in Amazonia: Causes, trends and impacts. *International Journal of Climatology*, 36(3), 1033-1050.

Marengo, J. A., Soares, W. R., Saulo, C., & Nicolini, M. (2004). Climatology of the low-level jet east of the Andes as derived from the NCEP-NCAR reanalyses: Characteristics and temporal variability. *Journal of Climate*, 17(12), 2261-2280.

McColl, K. A., Alemohammad, S. H., Akbar, R., Konings, A. G., Yueh, S., & Entekhabi, D. (2017). The global distribution and dynamics of surface soil moisture. *Nature Geoscience*, 10(2), 100-104.

Nepstad, D. C., de Carvalho, C. R., Davidson, E. A., Jipp, P. H., Lefebvre, P. A., Negreiros, G. H., da Silva, E. D., Stone, T. A., Trumbore, S. E., & Vieira, S. (1994). The role of deep roots in the hydrological and carbon cycles of Amazonian forests and pastures. *Nature*, 372(6507), 666-669.

Reichle, R. H., De Lannoy, G. J. M., Liu, Q., Ardizzone, J. V., Colliander, A., Conaty, A., Crow, W., Jackson, T. J., Jones, L. A., Kimball, J. S., Koster, R. D., & Mahanama, S. P. (2017). Assessment of the SMAP Level-4 surface and root-zone soil moisture product using in situ measurements. *Journal of Hydrometeorology*, 18(10), 2621-2645.

Ropelewski, C. F., & Halpert, M. S. (1987). Global and regional scale precipitation patterns associated with the El Nino/Southern Oscillation. *Monthly Weather Review*, 115(8), 1606-1626.

Stull, R. B. (1988). *An Introduction to Boundary Layer Meteorology*. Kluwer Academic Publishers, 666 pp.

Taylor, C. M., de Jeu, R. A. M., Guichard, F., Harris, P. P., & Dorigo, W. A. (2012). Afternoon rain more likely over drier soils. *Nature*, 489(7416), 423-426.

Taylor, C. M., et al. (2025). Wind shear enhances soil moisture influence on rapid thunderstorm growth. *Nature*, 651, 116-121. doi:10.1038/s41586-025-10045-7.

Taylor, C. M., Gounou, A., Guichard, F., Harris, P. P., Ellis, R. J., Couvreux, F., & De Kauwe, M. (2011). Frequency of Sahelian storm initiation enhanced over mesoscale soil-moisture patterns. *Nature Geoscience*, 4(7), 430-433.

Vera, C., Baez, J., Douglas, M., Emmanuel, C. B., Marengo, J., Meitin, J., Nicolini, M., Nogues-Paegle, J., Paegle, J., Penalba, O., Salio, P., Saulo, C., Silva Dias, M. A., Silva Dias, P., & Zipser, E. (2006). The South American Low-Level Jet Experiment. *Bulletin of the American Meteorological Society*, 87(1), 63-77.

Wang, C. (2002). Atlantic climate variability and its associated atmospheric circulation cells. *Journal of Climate*, 15(13), 1516-1536.

Watkins, M. M., Wiese, D. N., Yuan, D.-N., Boening, C., & Landerer, F. W. (2015). Improved methods for observing Earth's time variable mass distribution with GRACE using spherical cap mascons. *Journal of Geophysical Research: Solid Earth*, 120(4), 2648-2671.

Yoon, J.-H., & Zeng, N. (2010). An Atlantic influence on Amazon rainfall. *Climate Dynamics*, 34(2-3), 249-264.

Zemp, D. C., Schleussner, C.-F., Barbosa, H. M. J., Hirota, M., Montade, V., Sampaio, G., Staal, A., Wang-Erlandsson, L., & Rammig, A. (2017). Self-amplified Amazon forest loss due to vegetation-atmosphere feedbacks. *Nature Communications*, 8, 14681.

Figures

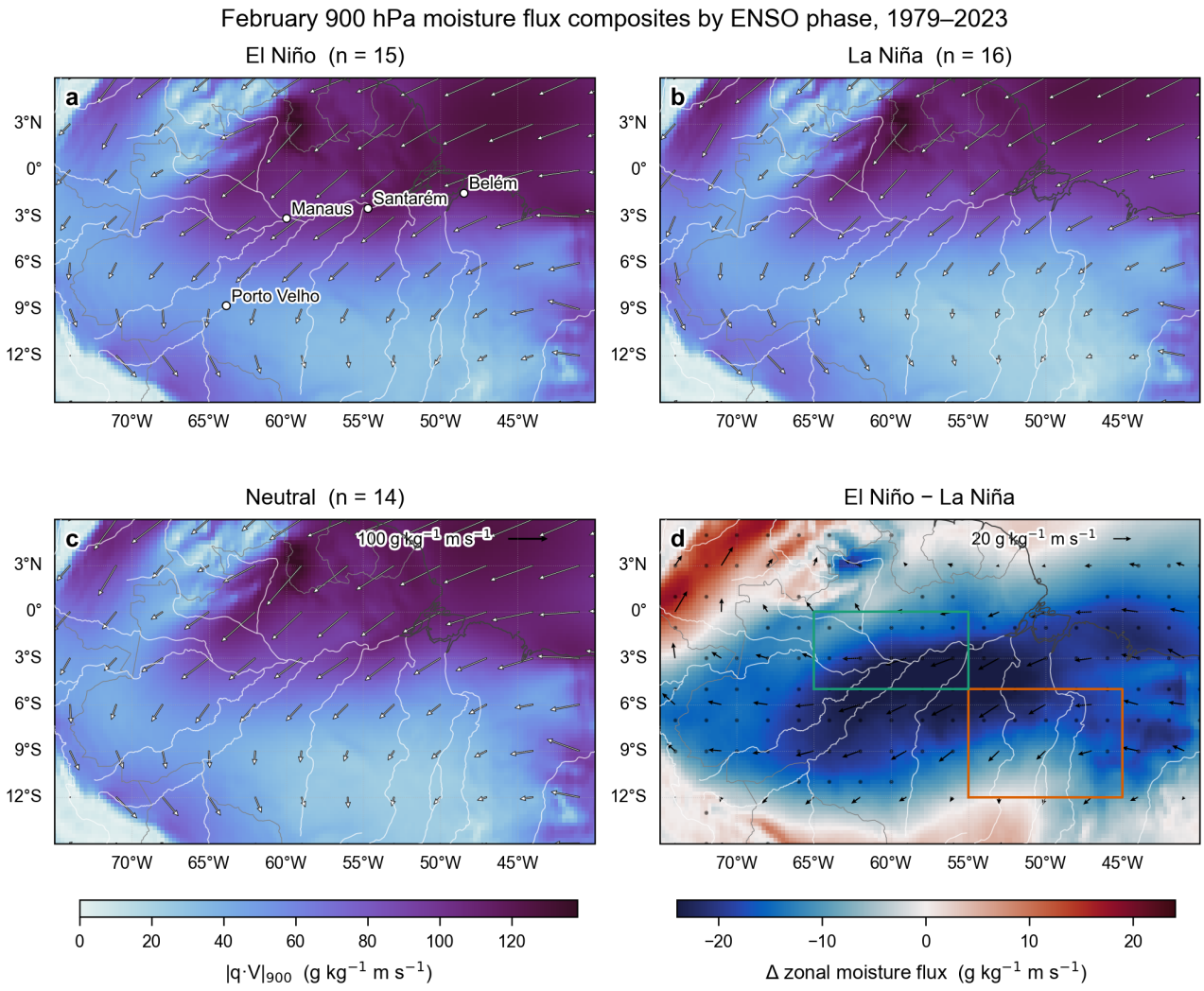

Figure 1: February 900 hPa moisture flux composites by ENSO phase, 1979–2023. (a) El Niño composite (n = 15); (b) La Niña composite (n = 16); (c) neutral composite (n = 14); (d) El Niño minus La Niña difference in zonal moisture flux, with stippling indicating statistical significance (Welch t-test, $p < 0.05$). Arrows show vector moisture flux at 900 hPa; shading shows flux magnitude (a–c) and zonal difference (d). Arc-of-deforestation (orange) and intact-interior (green) study sub-domains are outlined in panel (d).

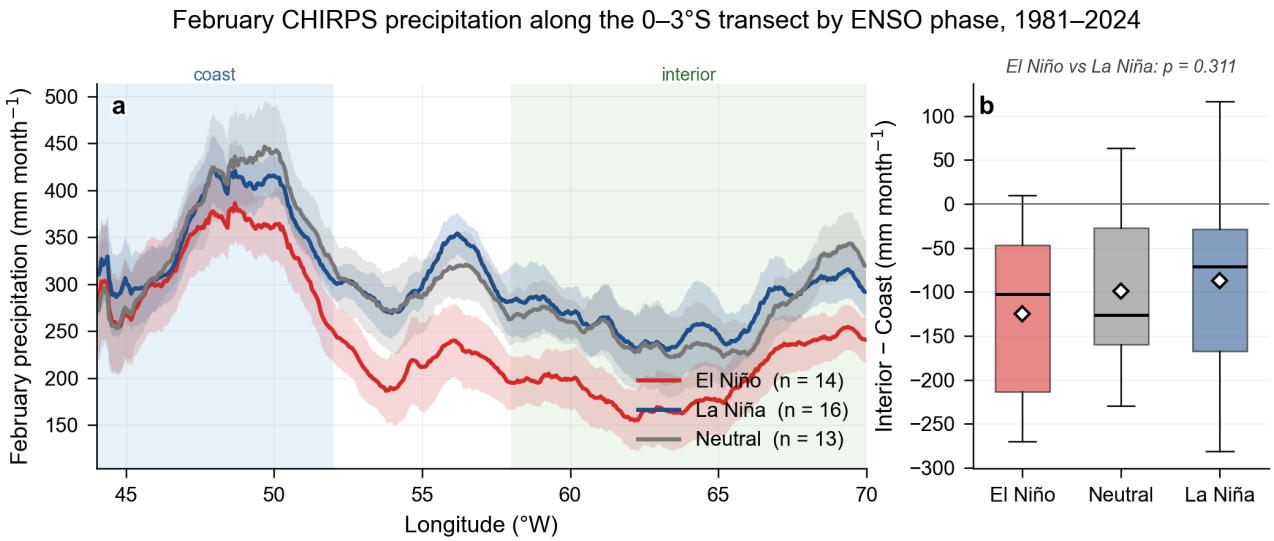

Figure 2: Coast-to-interior February precipitation transects (CHIRPS v2.0), 0–3°S band, 1981–2024. (a) Mean precipitation ± 1.96·SE for El Niño, La Niña, and neutral composites; coast (52–44°W) and interior (70–58°W) zones shaded. (b) Interior-minus-coast precipitation gradient by ENSO phase; box shows IQR + median, whiskers 1.5·IQR, diamond mean.

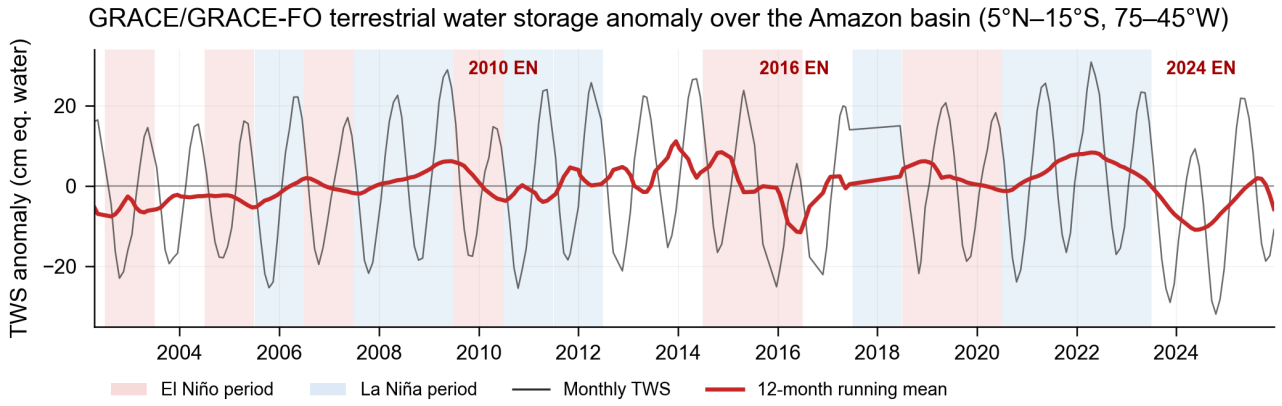

Figure 3: GRACE and GRACE-FO terrestrial water storage anomaly over the Amazon basin (5°N–15°S, 75–45°W), April 2002–December 2025. Thin line: monthly TWS; thick red line: 12-month running mean. Background shading marks El Niño (pink) and La Niña (blue) periods (Jul–Jun centred on each ENSO year). Major El Niño droughts (2010, 2016, 2024) labelled.

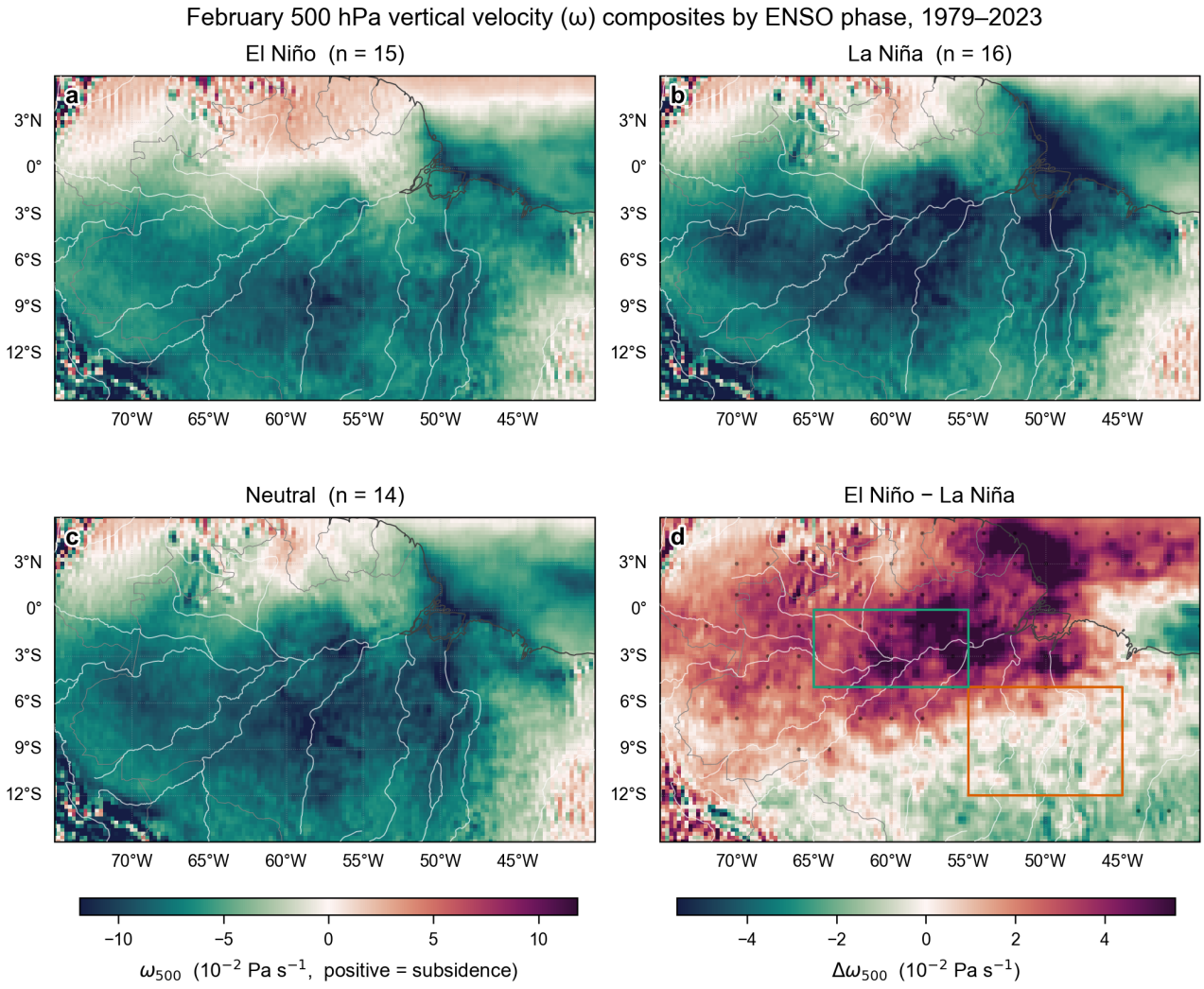

Figure 4: February 500 hPa vertical velocity (ω) composites by ENSO phase, 1979–2023. (a) El Niño (n = 15); (b) La Niña (n = 16); (c) neutral (n = 14); (d) El Niño minus La Niña difference, with stippling indicating Welch t-test $p < 0.05$. In ω convention, positive values indicate subsidence and negative values indicate ascent. Arc-of-deforestation and intact-interior sub-domains outlined in panel (d).

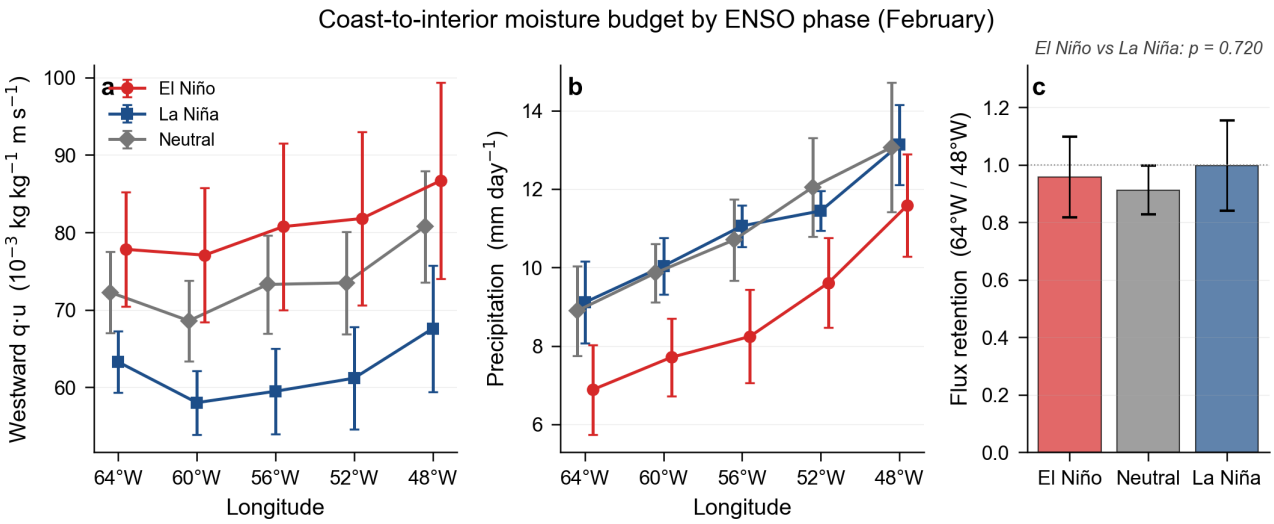

Figure 5: Coast-to-interior moisture budget by ENSO phase (February). (a) Westward 900 hPa moisture flux (q·u) at five transect longitudes from 64°W to 48°W, mean ± 1.96·SE. (b) CHIRPS precipitation at matching longitude bands, same units. (c) Flux retention ratio (64°W / 48°W) by phase; dotted line at 1.0 indicates no preferential coastal rain-out. El Niño vs La Niña Welch p-value annotated.

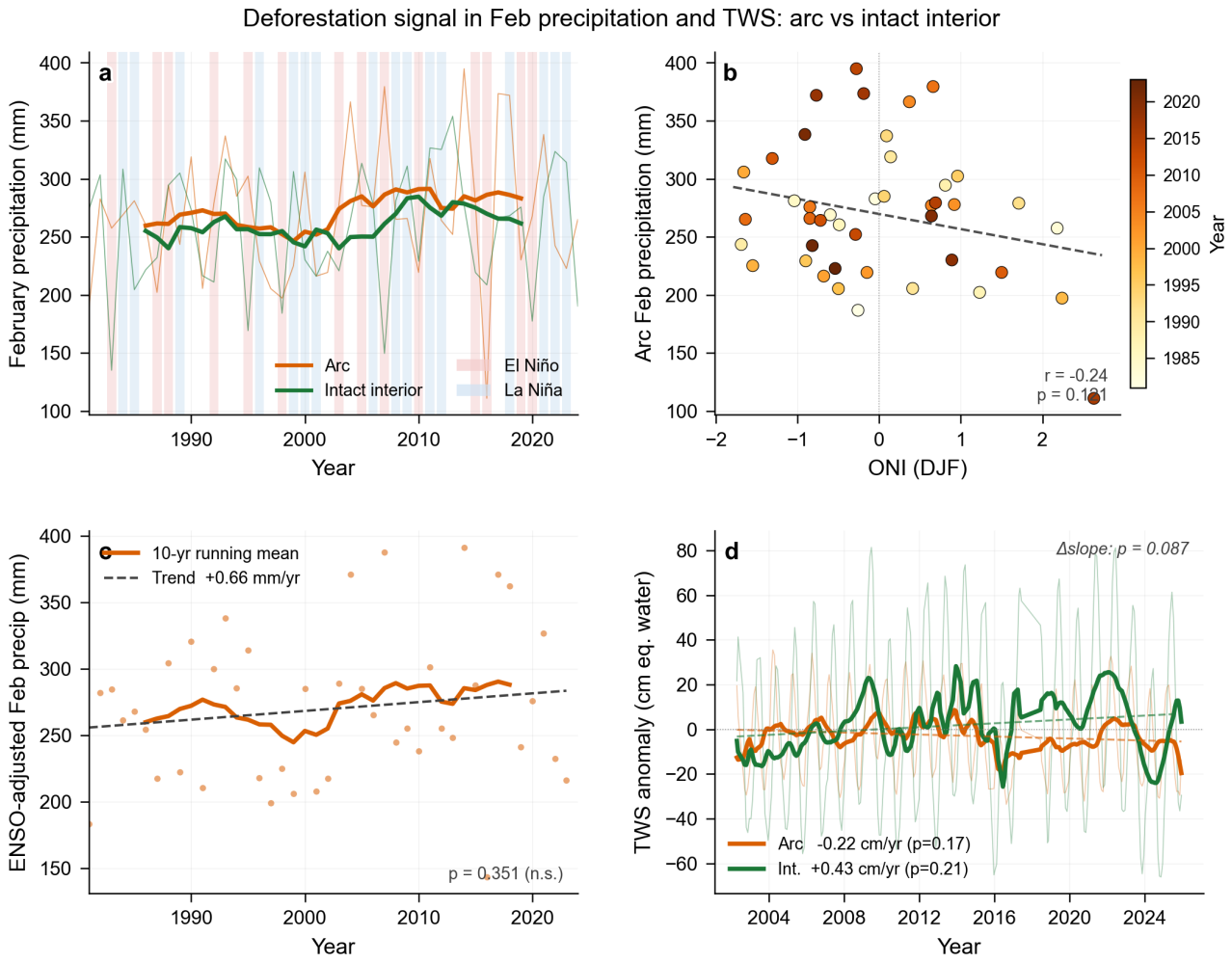

Figure 6: Deforestation signal in February precipitation and TWS — arc of deforestation vs intact interior. (a) Feb CHIRPS precipitation 1981–2024, 10-yr running means; ENSO years shaded. (b) ONI vs arc February precipitation; points coloured by year, with linear fit. (c) Residual arc precipitation after ENSO removal, with 10-yr running mean and secular trend. (d) GRACE TWS for the two regions with 12-month running means and linear trends; Δslope significance annotated.

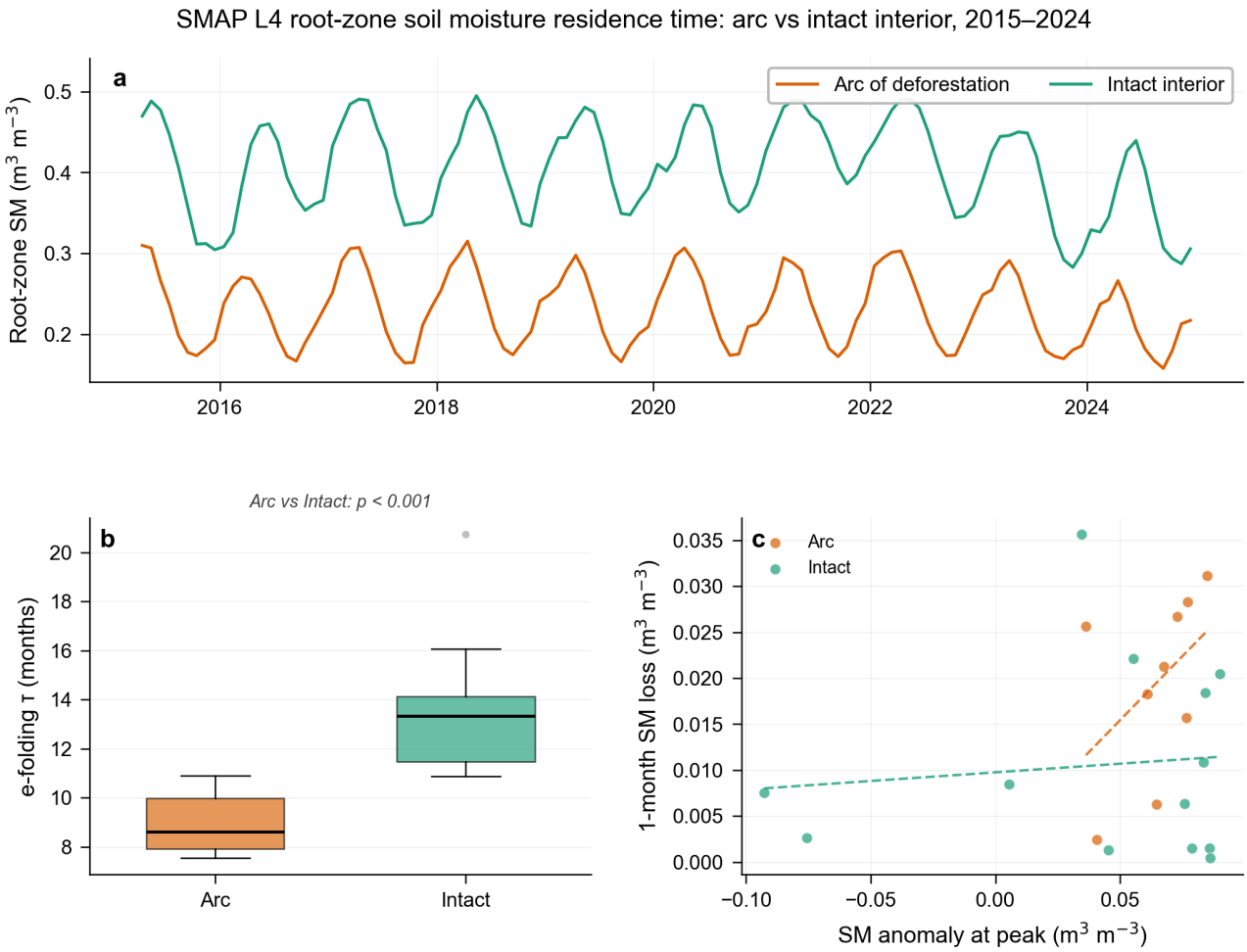

Figure 7: SMAP L4 (SPL4SMGP v8) root-zone soil moisture residence time, arc vs intact interior, 2015–2024. (a) Monthly root-zone soil moisture, arc and intact regions. (b) Exponential dry-down e-folding time τ from individual dry-down events; Welch t-test annotated. (c) SM anomaly at peak vs subsequent 1-month decay; dashed lines are linear fits.

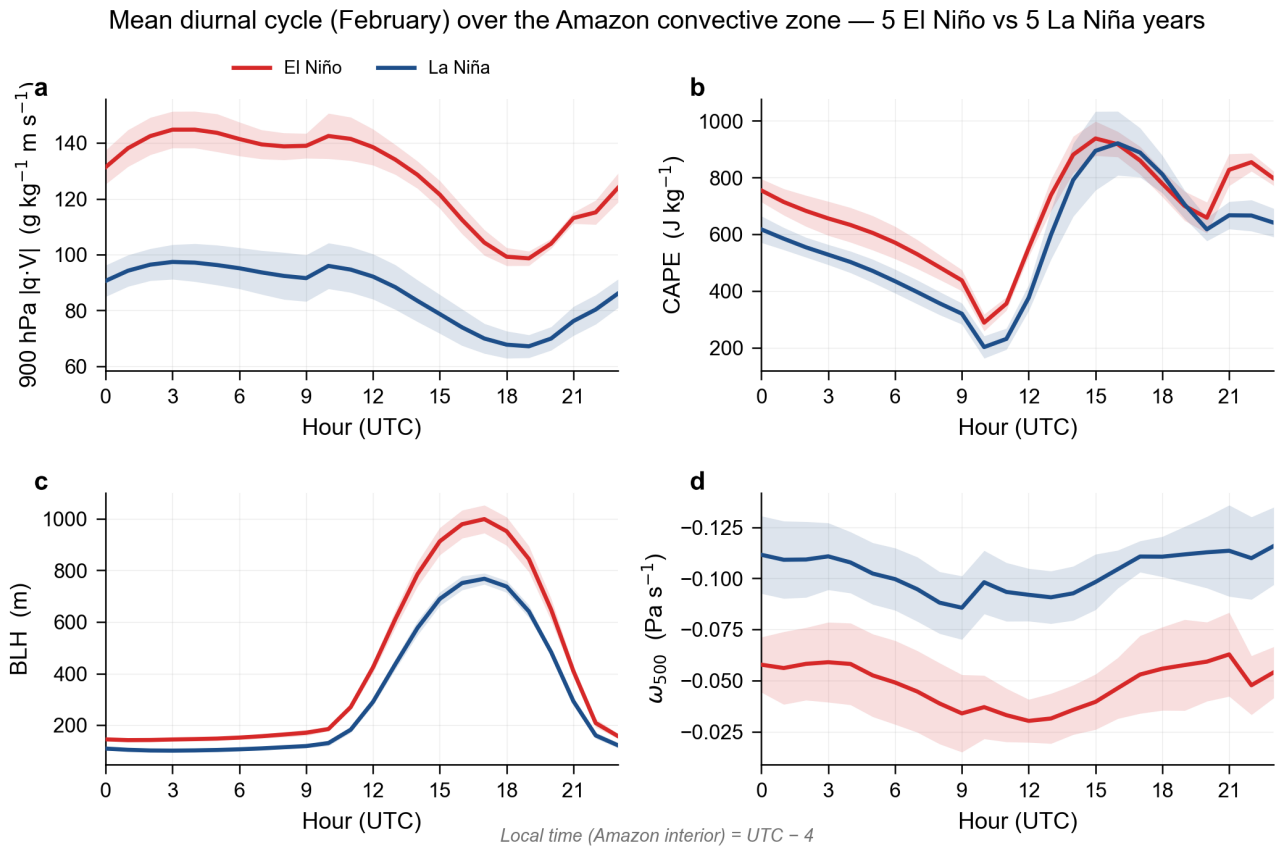

Figure 8: Mean diurnal cycle (February) over the Amazon convective zone (8–2°S, 60–50°W), composited across 5 El Niño and 5 La Niña Februaries. (a) 900 hPa moisture flux magnitude at 52°W (0–5°S); (b) area-mean CAPE; (c) area-mean boundary-layer height; (d) area-mean 500 hPa ω (y-axis inverted; ascent up). Shading is ±1σ across ENSO years. Local time = UTC − 4.

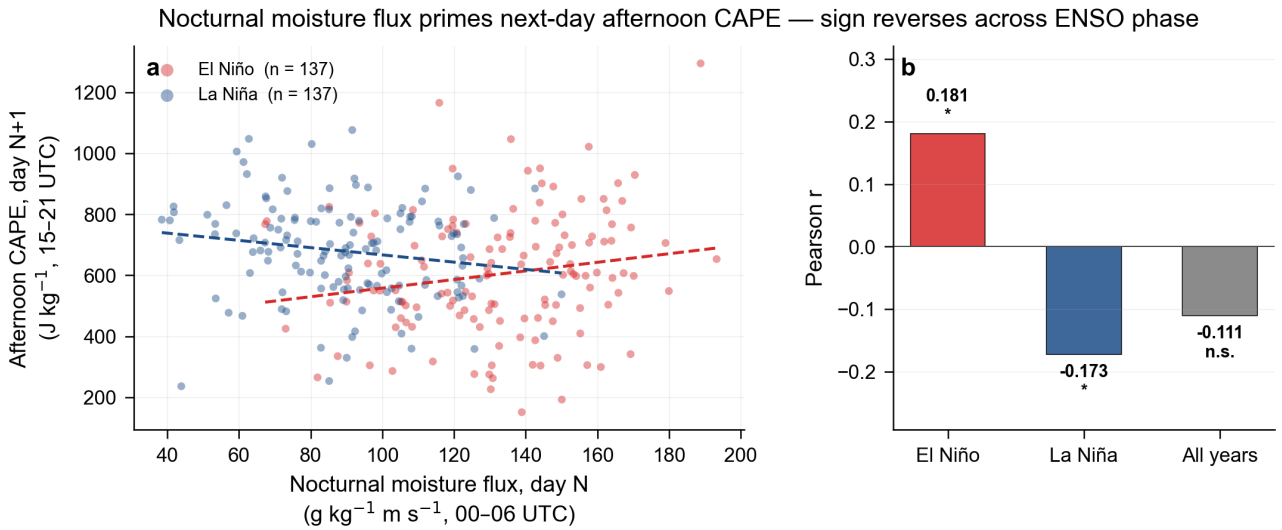

Figure 9: Nocturnal moisture flux primes next-day afternoon CAPE — sign reverses across ENSO phase. (a) Scatter of nocturnal mean 900 hPa moisture flux (day N, 00–06 UTC) vs afternoon CAPE on day N+1 (15–21 UTC), domain-averaged over 5–0°S, 60–50°W, separately for El Niño and La Niña days. Dashed lines are linear fits. (b) Pearson r for the El Niño, La Niña, and pooled-years correlations; significance marked (* $p < 0.05$).